SIAM J. APPL. MATH.
Vol. 75, No. 2, pp. 813–835

A HETEROGENEOUS MULTICLASS TRAFFIC FLOW MODEL WITH CREEPING*

SHIMAO FAN† AND DANIEL B. WORK‡

Abstract. A heterogeneous traffic model with two vehicle classes is developed to capture overtaking and creeping in highly heterogeneous traffic flows. Creeping is a special case of overtaking that occurs when small vehicles continue to advance in congestion even though larger vehicles have completely stopped. To motivate the new model, it is shown that a two class homogeneous multiclass model is equivalent to a class of second order models originally proposed by Aw, Rascle, and Zhang (ARZ). Based on the properties of the ARZ model, homogeneous models do not allow overtaking or creeping. The new creeping model is a phase transition model which applies a system of conservation laws in the noncreeping phase and a system equivalent to a scalar model in the creeping phase. The solution to the Riemann problem is obtained by investigating the elementary waves, particularly for the cases when one vehicle class is absent, as well as in the presence of a phase transition. Based on the proposed Riemann solver, the solution to the Cauchy problem is constructed using wavefront tracking. Numerical tests are carried out using a Godunov scheme to illustrate the creeping phenomenon. Source code for the numerical simulations is available at https://github.com/shimaof/heterogeneous-traffic-model.

Key words. hyperbolic system of conservation laws, macroscopic traffic flow model, heterogeneous flow, multiclass traffic model, phase transition, Riemann solver

AMS subject classifications. 35L65, 35F25, 90B20, 76T99

DOI. 10.1137/140977977

1. Introduction.

Consider a system-of-conservation-laws model of multiclass traffic flow in a general framework,

$$\begin{aligned} (\rho_j)_t + (\rho_j v_j)_x &= 0, \qquad j = 1, \dots, n, \\ v_j &= V_j(\vec{\rho}), \quad \text{with } \vec{\rho} = (\rho_1, \dots, \rho_n), \end{aligned} \tag{1.1}$$

which describes the conservation of vehicles for n vehicle classes indexed by j. Here, $\rho_j = \rho_j(x,t)$ is the traffic density of the jth class, which depends on both the location x and time t, and $V_j(\cdot)$ is the corresponding velocity function, which is a function of the density of each class. In the special case when $n = 1$, the system becomes the well-known *Lighthill–Whitham–Richards* (LWR) model [27, 33], and the flux function $Q(\rho) = \rho V(\rho)$ is a *fundamental diagram* (e.g., [19, 34]). Thus, the model (1.1) can be interpreted as a multiclass extension of the LWR model. The existing models for multiclass traffic flow that fit into framework (1.1) can be classified based on their assumptions on the interaction rules of different vehicle classes characterized by the specific form of the velocity functions $V_j(\cdot)$ (see Table 1).

1.1. Homogeneous multiclass models.

When all velocity functions are identical, i.e., $v_j = V(\vec{\rho})$, then (1.1) is a *homogeneous multiclass model* since all vehi-

*Received by the editors July 17, 2014; accepted for publication (in revised form) February 6, 2015; published electronically April 23, 2015. This work was supported in part by the National Science Foundation under grant 1351717.
http://www.siam.org/journals/siap/75-2/97797.html
†Coordinated Science Laboratory, University of Illinois at Urbana Champaign, Urbana, IL 61801 (shimao@illinois.edu). This author's work was partially supported by the California Department of Transportation under the PATH Connected Corridors program.
‡Department of Civil and Environmental Engineering and Coordinated Science Laboratory, University of Illinois at Urbana Champaign, Urbana, IL 61801 (dbwork@illinois.edu).

TABLE 1
Classification of multiclass models according to the definition of velocity functions.

	Model	Velocity v_j	Overtaking	Creeping
Homogeneous	Logghe & Immers [29]	$v_j = V\left(\sum_i \beta_i \rho_i\right)$	No	No
	Daganzo [12]	$v_j = V\left(\sum_i \rho_i\right)$	No	No
	Zhang & Jin [38]	$v_j = V\left(\rho_1, \rho_2\right)$	No	No
Heterogeneous	Ngoduy & Liu [32]	$v_j = V_j\left(\beta_j \sum_i \rho_i\right)$, with $v_j = V$ in congestion	Freeflow	No
	Fastlane [35]	$v_j = V_j\left(\sum_i \beta_i \rho_i\right)$, with $v_j = V$ in congestion	Freeflow	No
	Wong & Wong [36]	$v_j = V_j\left(\sum_i \rho_i\right)$	Yes	No
	Zhu et al. [40]	$v_j = v_j^{\mathrm{m}} V\left(\sum_i \rho_i\right)$	Yes	No
	n–populations [4]	$v_j = v_j^{\mathrm{m}} V\left(\sum_i \ell_i \rho_i\right)$	Yes	No
	Nair et al. [31]	$v_j = pV_{\mathrm{c}}(s) + (1-p)V_{\mathrm{f}}(s)$, $p = \int_0^{s_j} g(s)ds$, $g(s)$ is distribution of s	Yes	Yes
	Creeping model	$v_j = V_j\left(\sum_i \ell_i \rho_i\right)$, with $V_j(0) = v^{\mathrm{m}}$	Yes	Yes

cle classes follow the same kinematic behavior. These models are equivalent to the *Keyfitz–Kranzer* system [22] arising in elasticity theory. It is noted that homogeneous multiclass models are not strictly hyperbolic in general, with exceptions when $n \leq 2$ [4, 22].

An example of a homogeneous multiclass model is the *Logghe and Immers* model [29], which relates different vehicle classes by a scaling factor known as a *passenger car equivalent* (PCE). Accordingly, each class is modeled with a scaled fundamental diagram with a constant maximal speed, and the velocity function depends on a weighted sum of the densities of all vehicle classes, called the *effective density*. Hence, the velocity function is defined as $v_j = V\left(\sum_i \beta_i \rho_i\right)$, where β_i is the PCE applied to the ith class. A similar model of this form is Daganzo's 1-pipe special lane model [12]. Moreover, Zhang and Jin's model [38] can be treated as a special case of the Keyfitz–Kranzer system with $n = 2$. The *multicommodity model* [21] can also be classified as a two-class homogeneous multiclass model, where the two vehicle classes represent weaving and nonweaving vehicles.

Homogeneous multiclass models with $n = 2$ are also equivalent to a class of *second order models* originally proposed by Aw and Rascle [2] and Zhang [37] (ARZ) when the velocity is a strictly decreasing function of ρ_1 and ρ_2 (see section 2). The *source-destination model* [16] further applies the ARZ model to a road network, where the vehicle class is defined by the source and destination of the flow at a junction. A primary limitation of homogeneous models is that they do not allow one vehicle class to overtake another [4], which is an important feature for highly heterogeneous flows.

1.2. Heterogeneous multiclass models. Many research efforts are devoted to the design of *heterogeneous multiclass models* by distinguishing $V_j(\cdot)$ for each class. The model by Ngoduy and Liu [32] characterizes vehicle classes by their maximum velocities, and assumes that the freeflow velocity depends on a *PCE-scaled density*,

i.e., $v_j = V_j(\beta_j \sum_i \rho_i)$, where β_j is the PCE factor of the jth class. The model uses the same velocity function for all classes in congestion. The *Fastlane* model [35] also supposes that all vehicle classes have distinct velocity functions in freeflow but the same function in congestion; however, it defines the velocity as a function of the effective density (e.g., $v_j = V_j(\sum_i \beta_i \rho_i)$). As a consequence, the Ngoduy and Liu and Fastlane models [32, 35] allow overtaking in the freeflow regime but not in congestion.

Wong and Wong [36] introduced a simplified heterogeneous multiclass model of the form (1.1) that admits overtaking in freeflow and congestion. The velocity function of each class is a function of the *total density* (e.g., $v_j = V_j(\sum_i \rho_i)$), and they are distinct except at the jam density. The model of Zhu and Wu [40] also follows the same principle. Later, Benzoni-Gavage and Colombo [4] introduced the *n-populations model*, which extended Wong and Wong's model [36] by explicitly taking the size of each vehicle class into account. Instead of explicitly conserving the number of vehicles, the system expresses conservation of the space occupied by each vehicle class. Consequently, the velocity function depends on the *total occupied space* $r = \sum_j \ell_j \rho_j$, i.e., $v_j = V_j(r)$, where ℓ_j represents the average length of each vehicle class. As presented in [4], when $\hat{\rho}_j := \ell_j \rho_j$ is substituted into the n-populations model, both models [4, 36] fit into the same mathematical framework:

$$\begin{aligned} &(\hat{\rho}_j)_t + (\hat{\rho}_j v_j)_x = 0, \qquad j = 1, \dots, n, \\ &v_j = V_j(r), \quad \text{with } r = \sum_{j=1}^{n} \hat{\rho}_j. \end{aligned} \tag{1.2}$$

The models [4, 36, 40] suppose that all vehicle classes either never stop [36], or stop at a common *maximum occupied space* r^{m} (or equivalently an *effective jam density*), i.e., $V_j(r^{\mathrm{m}}) = 0$, $j = 1, \dots, n$. In circumstances when the vehicles are highly heterogeneous in size, this assumption may be violated. Indeed, one can observe that at a certain level of congestion, larger vehicles such as cars and buses completely stop, while small vehicles such as motorbikes continue to move through the gaps between the large vehicles. This *creeping* behavior can be interpreted as a special lane which can be used only by small vehicles.

Remark 1. The creeping phenomenon studied in this work is a special case of overtaking when the larger vehicle class is completely stopped. The new model not only allows overtaking in freeflow and congestion when both vehicle classes are moving, but also captures overtaking even through one vehicle class is stationary.

A heterogeneous multiclass model that allows for creeping is proposed by Nair, Mahmassani, and Miller-Hooks [31], which also fits into the generic framework (1.2). In this model, the velocity of each vehicle class is determined by the availability of empty spaces s (pores) for which vehicles of various sizes compete. Letting s_j represent a critical pore size for the jth class, vehicles may be in freeflow ($s \geq s_j$) or congestion ($s < s_j$) with velocity functions $V_{\mathrm{f}}(\cdot)$ and $V_{\mathrm{c}}(\cdot)$, respectively. The overall velocity of the jth class is

$$v_j = V_j(s) = \left(\int_{s_j}^{\infty} g(\omega) d\omega \right) V_{\mathrm{f}}(s) + \left(\int_{0}^{s_j} g(\omega) d\omega \right) V_{\mathrm{c}}(s), \tag{1.3}$$

where $g(\cdot)$ is the probability density function of the pore sizes for a given time, and $V_{\mathrm{c}}(s) \leq V_{\mathrm{f}}(s)$. The creeping property is shown by numerical simulations for a flow with two vehicle classes, but significant analytical results are missing due to the complexity

of the model (1.3); e.g., the density function $g(s)$ evolves with time. Interestingly, the model [31] reduces to a homogeneous multiclass model when $V_c(s) = V_f(s)$.

1.3. Outline and contributions. In this work, a new heterogeneous model is proposed with several important features: (i) it allows creeping, which permits small vehicles to move, even when large vehicles have completely stopped; (ii) it permits overtaking in the noncreeping phase; (iii) it is *anisotropic*, where information cannot travel faster than the fastest vehicle class; (iv) it is consistent with the LWR model when only one vehicle class is present; (v) it is well-posed away from the *vacuum*, i.e., the point where both vehicle classes disappear.

Well-posedness is an important property that has not been established for many heterogeneous models. The models that assign a unique maximum traffic velocity to each vehicle class [4, 36] have nonvacuum *umbilic points* where strict hyperbolicity is lost [4, 39]. Hence, they do not fit the standard conservation law theory (e.g., [7, 23, 24]), which leads to a challenge in proving the well-posedness of the system. This article presents a different way to distinguish velocity functions that enables creeping and moves the umbilic point to the vacuum. This simplifies the mathematical analysis considerably and allows for a well-posed system away from the vacuum.

The main contributions of this article include three aspects: (i) it is first shown that a two-class homogeneous multiclass model is an ARZ model, which completes the mathematical analysis associated with these models; (ii) a new two-class heterogeneous model that allows overtaking and creeping is introduced; and (iii) a comprehensive investigation of the properties of the new model is provided.

The remainder of the article is organized as follows. In section 2, a connection between the ARZ model and the homogeneous two-class models is introduced. Based on properties of the ARZ model, homogeneous multiclass models are not appropriate for overtaking. A new heterogeneous model for two vehicle classes is proposed, and its properties are outlined in section 3. The mathematical analysis of the model is presented in section 4, which includes verifying that the model is strictly hyperbolic away from the vacuum, investigating the elementary waves and using them to construct a Riemann solver, and providing a sketch of the proof of the well-posedness of the model. Section 5 is devoted to validating the features of the proposed model by performing numerical simulations and comparisons to the n-populations model.

2. Interpretation of a two-class homogeneous multiclass model as an ARZ model. As pointed out in [5, 14, 15], the ARZ model can be interpreted as a second order generalization of the LWR model, which allows for different vehicle properties such as aggressivity [13]. Recently, a generic framework based on the ARZ model has been presented [14, 25]:

$$
\begin{array}{lll}
(\rho)_t + (\rho v)_x = 0, & & (\rho)_t + (\rho v)_x = 0, \\
w_t + v w_x = 0, & \text{in conservation form} & (q)_t + (qv)_x = 0, \\
\text{where } v = V(\rho, w), & & \text{where } q = \rho w,\ v = V(\rho, q/\rho).
\end{array} \tag{2.1}
$$

Here, w represents a property of the traffic that is conserved along vehicle trajectories, and the velocity function $v = V(\rho, w)$, with $\partial_\rho V < 0$, generates a family of flow-density curves parametrized by w [14, 15]. Note that the condition $\partial_\rho V < 0$ is required to guarantee that system (2.1) is strictly hyperbolic for $\rho > 0$. In this framework, vehicles with the property w adjust their spacing $s = 1/\rho$ for a given velocity v, where ρ is determined such that $v = V(\rho, w)$. An aggressive driver tends to select a smaller space when traveling at the same speed as a passive driver.

Similarly, the various interaction behaviors among different classes in multiclass flow can also be interpreted as an assignment of road space to vehicle classes [30]. Hence, it is possible to link two-class heterogeneous models with the ARZ model. Consider a multiclass flow that is composed of cars ($j = 1$) and trucks ($j = 2$). By letting $\rho = (\rho_1 + \rho_2)$ be the total density and defining $w = \rho_1/\rho$ as the fraction of vehicles in the first class, the second equation in (2.1) is simply a conservation law for the first class, i.e., $q = \rho w = \rho_1$. Alternatively, one could define the property as the fraction of the second vehicle class, i.e., $w = \rho_2/\rho$, to generate a conservation law for the second vehicle class. Thus, the generic framework of (2.1) in its conservation form becomes

$$\begin{aligned} (\rho)_t + \left(\rho V\left(\rho, \rho_1/\rho\right)\right)_x &= 0, \\ (\rho_1)_t + \left(\rho_1 V\left(\rho_1, \rho_1/\rho\right)\right)_x &= 0. \end{aligned} \tag{2.2}$$

By subtracting the second equation from the first in (2.2), one obtains Zhang and Jin's [38] homogeneous two-class model,

$$\begin{aligned} (\rho_1)_t + \left(\rho_1 \tilde{V}(\rho_1, \rho_2)\right)_x &= 0, \\ (\rho_2)_t + \left(\rho_2 \tilde{V}(\rho_1, \rho_2)\right)_x &= 0, \end{aligned} \tag{2.3}$$

with $\tilde{V}(\rho_1, \rho_2) = V\left(\rho_1 + \rho_2, \rho_1/(\rho_1 + \rho_2)\right)$. Furthermore, one verifies that the requirement $\partial_\rho V < 0$ in the ARZ model is met under a sufficient condition:

$$\partial_{\rho_1} \tilde{V}(\rho_1, \rho_2) < 0 \quad \text{and} \quad \partial_{\rho_2} \tilde{V}(\rho_1, \rho_2) < 0. \tag{2.4}$$

Thus, a two class homogeneous multiclass model of the form (2.3) is equivalent to the ARZ model under the condition (2.4). Note that $v = V(\rho, w)$, $w = \rho_1/\rho$, generates a family of velocity curves that is parametrized by the fraction of cars. As the fraction of cars increases for a fixed total density ρ, the velocity curve shifts upwards.

Note also that Daganzo's 1-pipe special lane model [12] and the Logghe and Immers model [29] make the assumption that velocity depends only on the effective density, and therefore both models are special cases of (2.1). For example, in the Logghe and Immers model, a PCE β is applied such that $\rho = (\rho_1 + \beta\rho_2)$ with $w = \rho_1/\rho$, and $v = V(\rho_1 + \beta\rho_2) = V(\rho w + \rho(1 - w)) = V(\rho)$. Thus, in the Logghe and Immers model, the evolution of the density is not affected by the composition of the traffic flow.

An immediate consequence of these equivalent formulations is that all the analytical results of the ARZ model (e.g., [2, 25, 37]) transfer over to the models of the general form (2.3), provided that the velocity function is monotonically decreasing in the total density. This completes the mathematical analysis of homogeneous two-class models, e.g., the Logghe and Immers model [29]. Moreover, it also provides insights into why these models are inappropriate for modeling overtaking. Because the composition w is advected with the flow v, w cannot change faster than the speed of vehicles, which results in the first-in-first-out rule. This justifies the need for making distinctions in the velocity function among different vehicle classes in order to model overtaking behavior including creeping.

3. A new heterogeneous model with creeping.

3.1. Model outline. A new two-class model is proposed under the framework (1.2) in terms of occupied space $\hat{\rho}_j = \ell_j \rho_j$, which distinguishes r^{m} in each vehicle

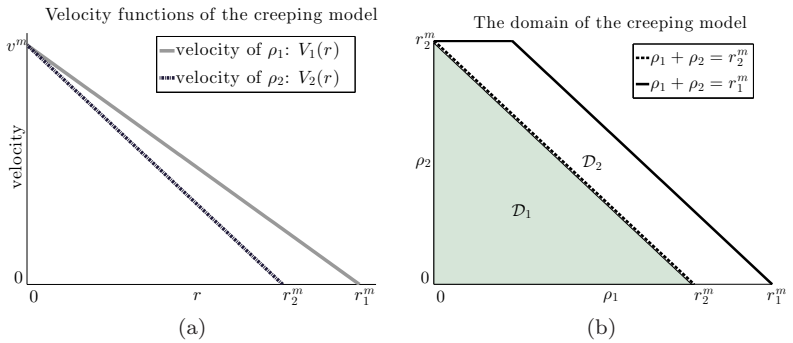

FIG. 1. (a) *Velocity functions of the creeping model* (3.5). *Here, the solid-gray line represents the velocity of the first vehicle class, and the dashed-blue line is the velocity of the second vehicle class.* (b) *The domain of the creeping model* (3.5).

class. By allowing r^{m} to vary between vehicle classes, the creeping phenomenon can be captured. For notational simplicity, let ρ_j represent the occupied space of the jth class, instead of using $\hat{\rho}_j$ in (1.2). Hence, $r = \rho_1 + \rho_2$ is the total occupied space. Suppose that the first class represents small creeping vehicles, and the second class is composed of large vehicles.

The new model is posed as a *phase transition model* [6, 9, 10] that considers two phases: a *noncreeping phase* and a *creeping phase*, which are defined as follows:

$$\mathcal{D}_1 = \left\{(\rho_1, \rho_2) \in \mathbb{R}^2 \mid \rho_j \geq 0,\ j = 1, 2;\ 0 < \rho_1 + \rho_2 < r_2^{\mathrm{m}}\right\},$$
$$\mathcal{D}_2 = \left\{(\rho_1, \rho_2) \in \mathbb{R}^2 \mid 0 \leq \rho_2 \leq r_2^{\mathrm{m}};\ r_2^{\mathrm{m}} \leq \rho_1 + \rho_2 \leq r_1^{\mathrm{m}}\right\}.$$

In $\mathcal{D}_1$, the model is a system of conservation laws, where the dynamics of both vehicle classes can be studied. In $\mathcal{D}_2$, the large vehicles are stationary at a time t, and thus the density remains unchanged; i.e., $(\rho_2)_t = 0$. In this case, the system reduces to the LWR model for ρ_1 with the possibility of discontinuous fluxes in space corresponding to shock profiles of ρ_2. Hence, in the special case that the density of one vehicle class is time invariant, the dynamics of a system of conservation laws can be described by a scalar conservation law. Thus, $\mathcal{D}_2$ represents a creeping phase, and $\mathcal{D}_1$ is a noncreeping phase (see Figure 1(b)). The model is written as

$$\begin{cases} \begin{cases} (\rho_1)_t + \left(\rho_1 V_1(r)\right)_x = 0 \\ (\rho_2)_t + \left(\rho_2 V_2(r)\right)_x = 0 \end{cases} & \text{if } (\rho_1, \rho_2) \in \mathcal{D}_1, \\ \begin{cases} (\rho_1)_t + \left(\rho_1 V_1(r)\right)_x = 0 \\ \text{with } (\rho_2)_t = 0 \end{cases} & \text{if } (\rho_1, \rho_2) \in \mathcal{D}_2, \end{cases} \tag{3.1}$$

where a phase change is defined between $\mathcal{D}_1$ and $\mathcal{D}_2$.

Here, the velocity functions $V_j(\cdot)$, $j = 1, 2$, have the following properties:

$$V_j'(r) < 0, \quad V_j(0) = v^{\mathrm{m}}, \quad V_1(r_1^{\mathrm{m}}) = V_2(r_2^{\mathrm{m}}) = 0, \quad r_2^{\mathrm{m}} < r_1^{\mathrm{m}} < 2r_2^{\mathrm{m}}, \tag{3.2}$$

where r_j^{m} are the maximum occupied spaces. Moreover, assume that the velocity functions are strictly decreasing, and both vehicle classes possess a common maximal speed v^{m} (see Figure 1(a)). The latter assumption is valid when the maximum velocities of different vehicle classes are restricted by a speed limit achievable by both

classes. The condition $r_1^{\mathrm{m}} < 2r_2^{\mathrm{m}}$ is a realistic condition on the maximum occupied space that simplifies the mathematical analysis.

Remark 2. The phase transition models [6, 9, 10] apply a scalar conservation law in freeflow and a system of conservation laws in congestion. In the creeping model (3.5), a system equivalent to a scalar model is employed in the creeping phase, and a system of conservation laws is applied in the noncreeping phase.

Remark 3. By construction, in this model creeping occurs whenever large vehicles are present and the total occupied space is greater than r_2^{m}, which is independent of the composition of vehicles. Consider an extreme case when only one or a few large vehicles are present in a dense stream of small vehicles such that $r > r_2^{\mathrm{m}}$. Clearly, the large vehicles would also move with the surrounding small vehicles. The current model cannot capture this behavior since the velocity of the large vehicles depends only on the total occupied space, i.e., $v_j = V_j(r)$. To prevent large vehicles stopping when a very dense flow is primarily composed of smaller vehicles, the velocity should depend on the density of each vehicle class explicitly, i.e., $v_j = V_j(\rho_1, \rho_2)$. This change increases the complexity of establishing properties of the model considerably compared to the present model, but represents an important future direction in the development of increasingly realistic creeping models.

The domain $\mathcal{D}$ of the model (3.1) is defined as a union of $\mathcal{D}_1$ and $\mathcal{D}_2$:

$$\mathcal{D} = \left\{(\rho_1, \rho_2) \in \mathbb{R}^2 \mid 0 \le \rho_j \le r_j^{\mathrm{m}},\ j = 1, 2;\ 0 < \rho_1 + \rho_2 \le r_1^{\mathrm{m}}\right\}, \tag{3.3}$$

which has a trapezoidal shape (see Figure 1(b)). Note that the vacuum is excluded from $\mathcal{D}$.

Based on the assumptions in (3.2), one may propose various velocity functions to generate multiclass fundamental diagrams, such as Drake's exponential model, the smooth three-parameter model [15], or the Greenshields model [19]. Note that some of these models may generate intersections between velocity curves for $r > 0$, which causes a loss of strict hyperbolicity away from the vacuum. This can be avoided depending on the choice of the free parameters in each model. For simplicity, the linear Greenshields model is used:

$$V_1(r) = v^{\mathrm{m}}(1 - r/r_1^{\mathrm{m}}), \qquad V_2(r) = v^{\mathrm{m}}(1 - r/r_2^{\mathrm{m}}). \tag{3.4}$$

The model (3.1) with Greenshields velocity functions (3.4) is written as

$$\begin{cases} \begin{cases} (\rho_1)_t + \left(\rho_1 v^{\mathrm{m}}(1 - (\rho_1 + \rho_2)/r_1^{\mathrm{m}})\right)_x = 0 \\ (\rho_2)_t + \left(\rho_2 v^{\mathrm{m}}(1 - (\rho_1 + \rho_2)/r_2^{\mathrm{m}})\right)_x = 0 \end{cases} & \text{if } (\rho_1, \rho_2) \in \mathcal{D}_1, \\ \begin{cases} (\rho_1)_t + \left(\rho_1 v^{\mathrm{m}}(1 - (\rho_1 + \rho_2)/r_1^{\mathrm{m}})\right)_x = 0 \\ \text{with} \quad (\rho_2)_t = 0 \end{cases} & \text{if } (\rho_1, \rho_2) \in \mathcal{D}_2. \end{cases} \tag{3.5}$$

By observing Figure 1(a), it is clear that the two velocity profiles intersect only at the vacuum. As shown later, this simplifies the analysis of the creeping model compared to intersections elsewhere in the domain. Because the velocity functions are linear, the deviation between the two velocity functions strictly increases with r. Alternative velocity functions may be considered to provide more control over the deviations and to potentially improve the predictive capabilities of the model. Moreover, one sees that the Greenshields model (3.4) generates a negative velocity for the second vehicle class for $r > r_2^{\mathrm{m}}$. The creeping model (3.5) successfully excludes the presence of this nonphysical negative velocity by applying a phase transition.

Remark 4. Another approach one may consider to avoid negative velocity in the second vehicle class while avoiding the need to pose the creeping model as a phase

transition model is to redefine the velocity function as

$$\tilde{V}_2(r) = \begin{cases} V_2(r) & \text{if } r \le r_2^{\mathrm{m}}, \\ 0 & \text{if } r_2^{\mathrm{m}} < r \le r_1^{\mathrm{m}}. \end{cases}$$

This approach is penalized by the loss of strict hyperbolicity for $r > r_2^{\mathrm{m}}$.

Note that (3.5) also reduces to the LWR model in the subdomain $\mathcal{D}_3 = \mathcal{D}_1 \cap (\{\rho_1 = 0\} \cup \{\rho_2 = 0\})$ when one vehicle class is absent. Accordingly, it is natural to use an LWR model in $\mathcal{D}_3$ and to define phase transitions between $\mathcal{D}_3$ and other domains. However, this approach significantly increases the complexity in constructing Riemann solutions among different phases. Moreover, it is unnecessary since the creeping model (3.5) is strictly hyperbolic in $\mathcal{D}_1$, and as shown in subsection 4.5, the creeping model is consistent with the LWR model in $\mathcal{D}_3$.

4. Model analysis. The ultimate goal of the analysis is to show that (3.5) is well-posed in $\mathcal{D}$, and that the solution is physically meaningful. Here, we analyze the model properties separately in $\mathcal{D}_1$ and $\mathcal{D}_2$. This analysis approach is valid because both domains are invariant, and moreover their union $\mathcal{D}$ is also invariant, as shown later in subsection 4.6.

Well-posedness of a system of conservation laws is shown in a general approach that is based on constructing a solution to the Riemann problem for (3.5) with piecewise constant initial data:

$$u(x,0) = \begin{cases} u^+ & \text{if } x > 0, \\ u^- & \text{if } x < 0, \end{cases} \tag{4.1}$$

where $u^- = \left(\rho_1^-, \rho_2^-\right)$ and $u^+ = \left(\rho_1^+, \rho_2^+\right)$ are initial states. Based on the Riemann solver, the existence theory follows from Glimm's random choice method [17, 28] and the wavefront tracking algorithm [1, 7, 8]. These techniques both require a strictly hyperbolic system of conservation laws. As a result, a first and key issue is to establish the hyperbolicity of the creeping model (3.5) in $\mathcal{D}_1$ and $\mathcal{D}_2$.

4.1. Hyperbolicity of the creeping model. First, the hyperbolicity of the model in $\mathcal{D}_1$ is established. The creeping model (3.5) in $\mathcal{D}_1$ is rewritten in a compact form,

$$u_t + f(u)_x = 0,$$

where $u = (\rho_1, \rho_2)$ is the vector of occupied space by class, and $f = (\rho_1 V_1(r), \rho_2 V_2(r))$ is the flux function. The *Jacobian* is calculated as

$$\mathbf{A} = \partial f(u) = \begin{pmatrix} V_1 + \alpha_1 & \alpha_1 \\ \alpha_2 & V_2 + \alpha_2 \end{pmatrix}, \tag{4.2}$$

where $\alpha_1 = \rho_1 V_1'$ and $\alpha_2 = \rho_2 V_2'$. Strict hyperbolicity of (3.5) in $\mathcal{D}_1$ is established in the following lemma.

LEMMA 4.1. *The creeping model* (3.5) *is strictly hyperbolic in* $\mathcal{D}_1$.

Proof. The model is strictly hyperbolic if and only if the Jacobian has two distinct eigenvalues. The characteristic polynomial of $\mathbf{A}$ is

$$P(\lambda) = \det(\mathbf{A} - \lambda \mathbf{I}) = \lambda^2 - (\kappa_1 + \kappa_2)\lambda + \kappa_1\kappa_2 - \alpha_1\alpha_2,$$

where $\kappa_j = v_j + \alpha_j$ and $\alpha_j \le 0$, $j = 1, 2$. It is easy to see that P always has two real roots because

$$\delta = (\kappa_1 - \kappa_2)^2 + 4\alpha_1\alpha_2 \ge 0;$$

thus, the system is hyperbolic. The only risk to lose strict hyperbolicity is when $\delta = 0$, which occurs when $\alpha_1 = 0$ and $V_1 = \kappa_2$, or $\alpha_2 = 0$ and $V_2 = \kappa_1$. These conditions hold only at the vacuum point, which does not belong to $\mathcal{D}_1$. Thus, λ_1 and λ_2 are distinct in $\mathcal{D}_1$, and the creeping model (3.5) is strictly hyperbolic in $\mathcal{D}_1$. ∎

Remark 5. Lemma 4.1 also holds for creeping models with velocity functions satisfying the conditions in (3.2).

The hyperbolicity of the creeping model (3.5) in $\mathcal{D}_2$ can also be established following the same procedure as Lemma 4.1 and is omitted for brevity.

Furthermore, the characteristic speeds of (3.5) in $\mathcal{D}$ are

$$\lambda_1 = 0.5\left(\kappa_1 + \kappa_2 - \sqrt{\delta}\right), \qquad \lambda_2 = 0.5\left(\kappa_1 + \kappa_2 + \sqrt{\delta}\right), \tag{4.3}$$

where $\lambda_1 < \lambda_2$. The left and right eigenvectors associated to each eigenvalue λ are

$$\ell_\lambda = \begin{pmatrix} \frac{1}{V_1-\lambda} \\ \frac{1}{V_2-\lambda} \end{pmatrix}, \qquad \gamma_\lambda = \begin{pmatrix} \frac{\alpha_1}{V_1-\lambda} \\ \frac{\alpha_2}{V_2-\lambda} \end{pmatrix}. \tag{4.4}$$

Note that the forms of the eigenvalues (4.3) and eigenvectors (4.4) are independent of the composition of vehicles.

The next lemma establishes that the creeping model (3.5) is anisotropic.

LEMMA 4.2. *The characteristic speeds* (4.3) *are bounded above by the fastest vehicle class:*

$$\max\{\lambda_1, \lambda_2\} \le \max\{V_1, V_2\}.$$

Proof. From (4.3) and the fact that $\alpha_j \le 0$, $j = 1, 2$, the bound for λ_1 is given as

$$\lambda_1 \le \min\{\kappa_1, \kappa_2\} \le \min\{V_1, V_2\} \le \max\{V_1, V_2\}.$$

For the second characteristic, one checks that

$$P\big(\max\{\kappa_1, \kappa_2\}\big) \le 0 \quad \text{and} \quad P\big(\max\{V_1, V_2\}\big) \ge 0.$$

By the intermediate value theorem, the bound for λ_2 is established:

$$\max\{\kappa_1, \kappa_2\} \le \lambda_2 \le \max\{V_1, V_2\}. \tag{4.5}$$

Both λ_1 and λ_2 are bounded above by $\max\{V_1, V_2\}$. ∎

Next, the analysis of the creeping model (3.5) in $\mathcal{D}_1$ is presented.

4.2. Property of the characteristic fields in $\mathcal{D}_1$. Next, it is shown that the hyperbolic system (3.5) fits the Lax framework [23] in $\mathcal{D}_1$. This is crucial for the construction of solutions to the Riemann problem, since it implies that the Riemann solver consists of simple waves (or *elementary waves*). By the definition of Lax [23], one needs to check that both characteristic fields $(\lambda(u), \gamma_\lambda(u))$ are either *genuinely nonlinear* ($\nabla\lambda(u) \cdot \gamma_\lambda(u) \neq 0$) or *linearly degenerate* ($\nabla\lambda(u) \cdot \gamma_\lambda(u) = 0$) for all u in $\mathcal{D}_1$. Here, $\nabla\lambda$ denotes the gradient of the function $\lambda(u)$. The following lemma verifies that the creeping model (3.5) is a Lax system in $\mathcal{D}_1$.

LEMMA 4.3. *Both characteristic fields of* (3.5) *are genuinely nonlinear in* $\mathcal{D}_1$.

Proof. The proof follows the procedure outlined in [4]. Instead of evaluating $\nabla\lambda \cdot \gamma_\lambda$ directly, one defines $\varphi_\lambda(\gamma_\lambda)$ as

$$\varphi_\lambda(\gamma_\lambda) = \ell_\lambda \cdot \nabla^2 f(u) \cdot (\gamma_\lambda, \gamma_\lambda) = (\nabla\lambda \cdot \gamma_\lambda)(\ell_\lambda \cdot \gamma_\lambda),$$

and checks whether $\varphi_\lambda(\gamma_\lambda)$ is nonzero, since $(\ell_\lambda \cdot \gamma_\lambda) \neq 0$. One calculates φ_λ as

$$\varphi_\lambda(\gamma_\lambda) = v^{\mathrm{m}}/r_1^{\mathrm{m}}(\lambda - V_2)\left(\left(\gamma_\lambda^{(1)}\right)^2 + \gamma_\lambda^{(1)}\gamma_\lambda^{(2)}\right) + v^{\mathrm{m}}/r_2^{\mathrm{m}}(\lambda - V_1)\left(\left(\gamma_\lambda^{(2)}\right)^2 + \gamma_\lambda^{(1)}\gamma_\lambda^{(2)}\right),$$

where $\gamma_\lambda^{(1)}$ and $\gamma_\lambda^{(2)}$ denote entries of the eigenvector γ_λ; i.e., $\gamma_\lambda = \left(\gamma_\lambda^{(1)}, \gamma_\lambda^{(2)}\right)$.

For the slower characteristic λ_1, it is clear that $\gamma_{\lambda_1}^{(1)}\gamma_{\lambda_1}^{(2)} \geq 0$ for the eigenvector γ_{λ_1} in (4.4). Moreover, from Lemma 4.2, one sees that $\varphi_{\lambda_1} < 0$ in $\mathcal{D}_1$. Thus, the first characteristic field is genuinely nonlinear in $\mathcal{D}_1$.

For the faster characteristic λ_2, φ_λ is rewritten as

$$\varphi_{\lambda_2}(\gamma_{\lambda_2}) = (\gamma_{\lambda_2}^{(1)} + \gamma_{\lambda_2}^{(2)})\left(v^{\mathrm{m}}/r_1^{\mathrm{m}}\gamma_{\lambda_2}^{(1)}(\lambda_2 - V_2) + v^{\mathrm{m}}/r_2^{\mathrm{m}}\gamma_{\lambda_2}^{(2)}(\lambda_2 - V_1)\right).$$

Thus, φ_{λ_2} vanishes if and only if

$$\gamma_{\lambda_2}^{(1)} + \gamma_{\lambda_2}^{(2)} = 0 \quad \text{or} \quad v^{\mathrm{m}}/r_1^{\mathrm{m}}\gamma_{\lambda_2}^{(1)}(\lambda_2 - V_2) + v^{\mathrm{m}}/r_2^{\mathrm{m}}\gamma_{\lambda_2}^{(2)}(\lambda_2 - V_1) = 0. \tag{4.6}$$

The first equality in (4.6) implies $\kappa_2 + \alpha_1 - \kappa_1 - \alpha_2 = 0$, which holds when $V_1 = V_2$. This implies that the second characteristic is genuinely nonlinear except at the point where two velocities coincide, i.e., at the vacuum.

Furthermore, the second equality of (4.6) gives

$$\lambda_2 = \frac{\kappa_2 V_1 + \kappa_1 V_2}{V_1 + V_2}. \tag{4.7}$$

Based on (4.5), it is clear that $\lambda_2 \geq \max\{\kappa_1, \kappa_2\}$. In contrast, (4.7) implies

$$\lambda_2 = \frac{\kappa_2 V_1 + \kappa_1 V_2}{V_1 + V_2} \leq \max\{\kappa_1, \kappa_2\},$$

so

$$\lambda_2 = \frac{\kappa_2 V_1 + \kappa_1 V_2}{V_1 + V_2} = \max\{\kappa_1, \kappa_2\}. \tag{4.8}$$

This further implies $\kappa_1 = \kappa_2$, in order for the second equality in (4.8) to hold. Moreover, by (4.3), $\lambda_2 = \max\{\kappa_1, \kappa_2\}$ implies $\alpha_1\alpha_2 = 0$. One solves for $\kappa_1 = \kappa_2$ and $\alpha_1\alpha_2 = 0$. The solution also lies at the vacuum. All together, $\varphi_{\lambda_2} = 0$ holds only at the vacuum, which is not in $\mathcal{D}_1$. Hence, the second characteristic field is also genuinely nonlinear in $\mathcal{D}_1$. ∎

4.3. Elementary waves in $\mathcal{D}_1$. Lemma 4.3 implies that the Riemann solution of the creeping model can be constructed from shocks or rarefactions in $\mathcal{D}_1$. To construct a Riemann solver, one needs to investigate the geometries of the Lax curves [23].

The Lax shock curves are computed from the *Rankine–Hugoniot* condition:

$$\sigma(u^+ - u^-) = f(u^+) - f(u^-), \tag{4.9}$$

where $\sigma \in \mathbb{R}$ is the speed of the shock. To obtain an admissible solution in the presence of a shock, the *Lax entropy condition* [23] should be met:

$$\lambda_j\left(u^+\right) \leq \sigma_j \leq \lambda_j\left(u^-\right), \qquad j = 1, 2, \tag{4.10}$$

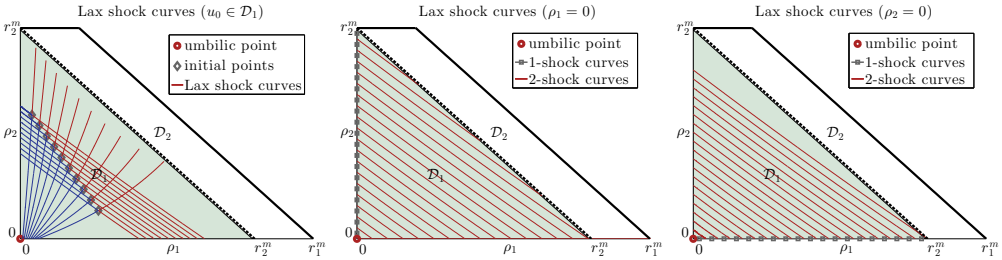

FIG. 2. *Lax shock curves starting at $u_0 \in \mathcal{D}_1$. (a) The case when u_0 is interior of $\mathcal{D}_1$. (b) The case with u_0 on the ρ_2-axis. (c) The case with u_0 on the ρ_1-axis. In* (a)*, the curves with $r > \rho_1^0 + \rho_2^0$ are marked as red, and those with $r < \rho_1^0 + \rho_2^0$ are in blue. In* (b) *and* (c)*, 1-shock curves (gray curves with square markers) remain in $\mathcal{D}_3$ and coincide with the ρ_2-axis and ρ_1-axis, respectively; the 2-shock curves (solid-red) are convex and monotonic.*

where λ_j and σ_j are the characteristic and the shock speed of the jth family.

The Lax rarefaction curves are the integral curves of the eigenvectors. Note that one can choose various eigenvectors. For simplicity, consider those introduced in [4]:

$$\gamma_{\lambda_1} = \begin{pmatrix} \lambda_1 - \kappa_2 + \alpha_1 \\ \lambda_1 - \kappa_1 + \alpha_2 \end{pmatrix}, \qquad \gamma_{\lambda_2} = \begin{pmatrix} -\lambda_2 + \kappa_2 + \alpha_1 \\ \lambda_2 - \kappa_1 - \alpha_2 \end{pmatrix}. \tag{4.11}$$

These eigenvectors have the advantage of being genuine eigenvectors, i.e., nonvanishing in $\mathcal{D}$. By Lemma 4.2, one sees that

$$\gamma_{\lambda_1}^{(1)} \le 0, \quad \gamma_{\lambda_1}^{(2)} \le 0; \qquad \gamma_{\lambda_2}^{(1)} \le 0, \quad \gamma_{\lambda_2}^{(2)} \ge 0. \tag{4.12}$$

4.3.1. Geometry of the lax shock curves. From the Rankine–Hugoniot condition (4.9), Lax shock curves starting from an initial state $u_0 = (\rho_1^0, \rho_2^0)$ are

$$\rho_1 (V_1 - \sigma) = \rho_1^0 \left(V_1^0 - \sigma\right), \qquad \rho_2 (V_2 - \sigma) = \rho_2^0 \left(V_2^0 - \sigma\right), \tag{4.13}$$

where $V_1^0 = V_1\left(\rho_1^0 + \rho_2^0\right)$ and $V_2^0 = V_2\left(\rho_1^0 + \rho_2^0\right)$. By solving for σ in the first equation of (4.13), and substituting it into the second equation, (4.13) can be rewritten as

$$\rho_2\left((\rho_1 - \rho_1^0)V_2 - \left(\rho_1 V_1 - \rho_1^0 V_1^0\right)\right) = \rho_2^0\left((\rho_1 - \rho_1^0)V_2^0 - \left(\rho_1 V_1 - \rho_1^0 V_1^0\right)\right). \tag{4.14}$$

Thus, Lax shock curves starting at u_0 are represented as

$$\mathcal{H}(u_0) = \left\{(\rho_1, \rho_2) \in \mathbb{R}^2 \mid \text{ s.t. (4.14) holds}\right\}.$$

If $u_0 \in \mathcal{D}_1 \setminus \mathcal{D}_3$, then (4.14) is a hyperbola, which is convex and monotonic in the interior of $\mathcal{D}_1$. Moreover, 1-shock curves are strictly increasing, while 2-shock curves are strictly decreasing and exit from the ρ_1-axis (see Figure 2(a)).

When $u_0 \in \mathcal{D}_3$, e.g., on the ρ_2-axis, (4.14) implies either $\rho_1 = 0$ or $\sigma = V_1$. In the former case, (4.14) reduces to the Rankine–Hugoniot condition for an LWR model applied to the second vehicle class. This is a 1-shock curve that coincides with the ρ_2-axis. In the latter case, the shock speed is the same as the velocity of the first vehicle class $\sigma = V_1$. The hyperbola (4.14) for 2-shock curves becomes

$$(r_2^{\mathrm{m}} - r_1^{\mathrm{m}})\,\rho_2\,(\rho_1 + \rho_2) - r_2^{\mathrm{m}}\rho_2^0\,(\rho_1 + \rho_2) + r_1^{\mathrm{m}}\rho_2^0\left(\rho_1^0 + \rho_2^0\right) = 0,$$

which is convex, monotonic, and exits from the boundary $\rho_2 = 0$ (see Figure 2(b)). The analysis of the case when u_0 is on the ρ_1-axis follows the same process, in which 1-shock curves coincide with the ρ_1-axis, and 2-shock curves are convex and monotonic, exiting from the boundary $\rho_1 = 0$ (see Figure 2(c)).

4.3.2. Geometry of the Lax rarefaction curves. The lemma below gives the properties for the Lax rarefaction curves. Note that it is not possible to derive an equation for the rarefaction curves due to the complexity of the eigenvalues and eigenvectors in the creeping model. Instead, in order to study the properties of the rarefaction curves, the techniques applied in [4] are used.

LEMMA 4.4. (i) *the Lax rarefaction curves of* (3.5) *defined by* (4.11) *are monotonic and convex in* $\mathcal{D}_1 \backslash \mathcal{D}_3$*; moreover,* (ii) *the* 1*-rarefaction curves are monotonically increasing, while the* 2*-rarefaction curves are monotonically decreasing in* $\mathcal{D}_1 \backslash \mathcal{D}_3$*; and* (iii) *in* $\mathcal{D}_3$*,* 1*-rarefaction curves coincide with the* ρ_1*-axis and* ρ_2*-axis. In contrast,* 2*-rarefaction curves coincide only with the* ρ_2*-axis.*

Proof. First, the monotonicity of the Lax rarefaction curves follows from (4.12). To show the concavity properties of the rarefaction curves, it is noted that the curvature of an integral curve is positively proportional to $\gamma_{\lambda_j} \wedge (\nabla \gamma_{\lambda_j} \cdot \gamma_{\lambda_j})$ [4], where " $\wedge$ " represents the exterior product. One calculates that

$$\gamma_{\lambda_j} \wedge (\nabla \gamma_{\lambda_j} \cdot \gamma_{\lambda_j}) = \frac{2(a_1 - a_2)}{(\lambda_j - V_2)\gamma_{\lambda_j}^{(1)} + (\lambda_j - V_1)\gamma_{\lambda_j}^{(2)}} (\lambda_j - V_1)\gamma_{\lambda_j}^{(1)}\gamma_{\lambda_j}^{(2)} \left(\gamma_{\lambda_j}^{(1)} + \gamma_{\lambda_j}^{(2)}\right).$$

Here, $a_j = v^{\mathrm{m}}/r_j^{\mathrm{m}}$, and $a_1 < a_2$ by (3.2). Moreover, one can check that in $\mathcal{D}_1$

$$\gamma_{\lambda_j} \wedge (\nabla \gamma_{\lambda_j} \cdot \gamma_{\lambda_j}) \le 0, \qquad j = 1, 2. \tag{4.15}$$

By the definition of the eigenvectors (4.12), one sees that the curvature center of each integral curve lies above the integral curve, which implies that the rarefaction curves are convex.

Moreover, these curves have zero curvature if the equality in (4.15) holds:

$$\gamma_{\lambda_j}^{(1)} + \gamma_{\lambda_j}^{(2)} = 0 \quad \text{or} \quad \lambda_j = V_1 \quad \text{or} \quad \gamma_{\lambda_j}^{(1)} = 0 \quad \text{or} \quad \gamma_{\lambda_j}^{(2)} = 0. \tag{4.16}$$

For the 1-rarefaction curves, the conditions in (4.16) are equivalent to

$$\rho_1 = 0, \quad \rho_2 > 0 \qquad \text{or} \qquad \rho_2 = 0, \quad \rho_1 > 0.$$

In other words, 1-rarefaction curves starting from a point in $\mathcal{D}_3$ remain in $\mathcal{D}_3$.

For the 2-rarefaction curves, the equality $\lambda_2 = V_1$ in (4.16) gives $\rho_1 = 0,\ \rho_2 > 0$, and the other equalities in (4.16) are not possible for the creeping model (3.5) in $\mathcal{D}_1$. Thus, the 2-rarefaction curves starting from a point lying on the ρ_2-axis coincide with the ρ_2-axis. When starting from a point on the boundary $\rho_2 = 0$, the rarefaction curves are convex, monotonic, and exit the boundary $\rho_1 = 0$. ∎

Note that a loss of symmetry is present in the last statement of Lemma 4.4. The 1-rarefaction curves coincide with both the ρ_1-axis and the ρ_2-axis, while 2-rarefaction curves coincide only with the ρ_2-axis. While symmetry is expected in ARZ-type models, heterogeneous multiclass models may not have symmetry (cf. [4]).

Based on the discussion in previous sections, the properties of the Lax curves in $\mathcal{D}_1$ have been established. To assure admissible solutions, the Lax entropy condition (4.10) must be satisfied for shock and rarefaction solutions [4, 39]. In particular, the

total occupied space r increases along a shock curve, i.e., $\rho_1^- + \rho_2^- < \rho_1^+ + \rho_2^+$. In contrast, rarefaction curves connect a higher r on the upstream to a lower one on the downstream, i.e., $\rho_1^- + \rho_2^- > \rho_1^+ + \rho_2^+$. Hence, the Lax curves that violate the entropy condition are truncated. For instance, 2-shock curves starting at the boundary $\rho_2 = 0$ connect to smaller r values (see Figure 2(c)); thus, these curves are not admissible.

In summary, the properties of elementary waves for the model are studied in $\mathcal{D}_1$. It remains to analyze the model in the creeping phase $\mathcal{D}_2$, where the creeping model reduces to an LWR model for the first vehicle class, and ρ_2 is stationary.

4.4. Model analysis in $\mathcal{D}_2$. In $\mathcal{D}_2$, the creeping model is rewritten as

$$(\rho_1(x,t))_t + \big(f_1(\rho_2(x), \rho_1(x,t))\big)_x = 0, \tag{4.17}$$

where the flux function $f_1 = \rho_1 v^{\mathrm{m}}(1-(\rho_1+\rho_2)/r_1^{\mathrm{m}})$ is smooth in ρ_1 and ρ_2, and $\rho_2(x)$ is a bounded integrable function with a possibly infinite number of discontinuities. The well-posedness of a hyperbolic conservation law model in the form of (4.17) with initial data in $\boldsymbol{L^1 \cap L^\infty}$ is established in [3]. Thus, the creeping model is well-posed in $\mathcal{D}_2$, given that the initial data of the creeping phase belongs to $\boldsymbol{L^1 \cap L^\infty}$. Based on the strict hyperbolicity and the characteristics of the elementary waves of the model in the noncreeping phase, it is guaranteed that the solutions transitioning from $\mathcal{D}_1$ that serve as the initial data for the creeping phase belong to $\boldsymbol{L^1 \cap L^\infty}$.

4.5. Riemann solver in $\mathcal{D}$. Recall that the Riemann problem is the building block for constructing a weak solution to the Cauchy problem for hyperbolic conservation laws. Due to the difficulty in obtaining the *Riemann invariant* [7, 23, 24] associated with each characteristic field in heterogeneous multiclass models, it is extremely difficult to construct an explicit Riemann solver [4, 39]. Alternatively, the existence and uniqueness of a solution to the Riemann problem is established based on the existing theories. Moreover, as shown later in section 5.1, the lack of an exact Riemann solver does not cause a problem in the numerical solver.

Following the standard theory for hyperbolic conservation laws, a general solution to the Riemann problem with piecewise constant initial states (4.1) is defined by first connecting the left state u^- to an intermediate state u^* with curves of the first family (the 1-Riemann invariant is constant along 1-Lax curves), and then connecting u^* to the right state u^+ with curves of the second family (the 2-Riemann invariant is constant along 2-Lax curves).

When both initial states are in $\mathcal{D}_1$, one constructs a unique Riemann solution based on the structure of the Lax curves [23]. Here, it is important to verify that the solutions are physically meaningful. In $\mathcal{D}_3$, an example that gives nonphysical solutions is considered in the n-populations model [4]. Given an initial condition with no vehicles of the second type, the solution to the Riemann problem produces an intermediate state (ρ_1^*, ρ_2^*) with the presence of the second class, i.e., $\rho_2^* > 0$. This is clearly incorrect because the second vehicle class appears in the solution when initially it did not exist. The correct solution should be $\rho_2^* = 0$, and the Riemann solution should be consistent with the LWR model. The issue illustrated in this example [4] is due to the loss of strict hyperbolicity in the n-populations model.

One verifies that the creeping model (3.5) is consistent with the LWR model when only one vehicle class is present. Based on the investigations of the properties of the Lax curves in section 4.3, 1-Lax curves remain in $\mathcal{D}_3$. Therefore, it is clear that Riemann solutions are consistent with those of the LWR model.

When u^- and u^+ are in $\mathcal{D}_2$, a Riemann problem for the LWR model is solved (see, e.g., [26]). Thus, to complete the Riemann solver in $\mathcal{D}$, it remains to define a

solution for phase transitions between $\mathcal{D}_1$ and $\mathcal{D}_2$. Consider the Riemann problem (4.1) with $u^- \in \mathcal{D}_2$ and $u^+ \in \mathcal{D}_1$. In order to construct a Riemann solution with phase transition, one needs to find intermediate states u^* based on the elementary waves. Thus, a Riemann solution with two intermediate states is defined:

1. A phase transition is defined by connecting $u^- = (\rho_1^-, \rho_2^-)$ to the phase boundary $\rho_1+\rho_2 = r_2^{\mathrm{m}}$ along a curve that is parallel to the ρ_1-axis. It is a rarefaction curve in the conservation equation for the first vehicle class. This intermediate state can be solved explicitly as $u_1^* = (r_2^{\mathrm{m}} - \rho_2^-, \rho_2^-)$.
2. The second intermediate state u_2^* is constructed for a hyperbolic system with two initial states u_1^*, $u^+ \in \mathcal{D}_1$.

The construction of a Riemann solution with $u^+ \in \mathcal{D}_2$ and $u^- \in \mathcal{D}_1$ follows the same procedure.

4.6. Invariance of $\mathcal{D}$. To guarantee a physical Riemann solution [2], one verifies that $\mathcal{D}$ in (3.3) is an *invariant region* for the Riemann problem. For convenience, the invariance of the two subdomains $\mathcal{D}_1$ and $\mathcal{D}_2$ is shown, and then the cases in the presence of a phase transition are considered.

First, it is easy to check that $\mathcal{D}_1$ is invariant since the creeping model (3.5) meets the sufficient conditions proposed by Hoff [20]. Second, the domain $\mathcal{D}_2$ is invariant. This is because the Lax curves in $\mathcal{D}_2$ are parallel to the ρ_1-axis, and thus the Riemann solution remains in $\mathcal{D}_2$ given both initial states in $\mathcal{D}_2$. Finally, in the presence of a phase transition, the Riemann solution also remains in $\mathcal{D}$ (see section 4.5). It is concluded that $\mathcal{D}$ is invariant. By the invariance of domains, phase transitions never occur when both initial states are in the same subdomain, either $\mathcal{D}_1$ or $\mathcal{D}_2$.

Remark 6. The invariance of $\mathcal{D}$ excludes the appearance of an intermediate vacuum state, which exists, for example, in the ARZ model [2, 14].

By the Riemann solver described in section 4.5, the Riemann solution always depends continuously on the initial data, even with the presence of phase transitions. Therefore, it can be verified that the size of the wave that connects two initial states $\sum(u^-, u^+)$ of a Riemann problem is bounded:

$$c \cdot \|u^+ - u^-\| \le \sum (u^-, u^+) \le C \cdot \|u^+ - u^-\|, \tag{4.18}$$

where c and C are given constants.

Next, the well-posedness of the Cauchy problem for the creeping model in $\mathcal{D}$ is established.

4.7. Cauchy problem. Following the theories of phase transition models in [6, 9, 10], a weak solution to the Cauchy problem of the system (3.5) is defined following a standard formulation. In particular, the fluxes on the left and right states are defined when there is a phase change:

$$f^- = \begin{cases} \sum_j \rho_j^- V_j(\rho_1^- + \rho_2^-) & \text{if } (\rho_1^-, \rho_2^-) \in \mathcal{D}_1, \\ \rho_1^- V_1(\rho_1^- + \rho_2^-) & \text{if } (\rho_1^-, \rho_2^-) \in \mathcal{D}_2, \end{cases}$$

$$f^+ = \begin{cases} \sum_j \rho_j^+ V_j(\rho_1^+ + \rho_2^+) & \text{if } (\rho_1^+, \rho_2^+) \in \mathcal{D}_1, \\ \rho_1^+ V_1(\rho_1^+ + \rho_2^+) & \text{if } (\rho_1^+, \rho_2^+) \in \mathcal{D}_2, \end{cases}$$

where the Rankine–Hugoniot condition (4.9) must be satisfied:

$$\sigma \cdot \left(\sum_j \rho_j^+ - \sum_j \rho_j^- \right) = f^+ - f^-.$$

The existence of an admissible solution to the Cauchy problem of the creeping model (3.5) is proved by a standard wavefront tracking procedure [1, 7, 8]. Here, a sketch of the proof is provided. Given a piecewise constant initial state with small total variation, the front tracking algorithm defines a sequence of piecewise constant approximations $(u_k)_{k>1}$ by piecing together Riemann solutions at each interface where two fronts interact for each time step. Based on (4.18), one sees that the total variation of $u_k(\cdot, t)$ is bounded uniformly for arbitrary initial states with small total variation. Finally, following the Glimm scheme [17, 28], one can construct a subsequence of approximation solutions that converges to a unique admissible weak solution, which depends continuously on initial data in $\mathcal{D}$.

4.8. Vacuum problem. The mathematical analysis of the previous sections is restricted to $\mathcal{D}$, which excludes the vacuum. In practice, vacuum initial states are physically meaningful, e.g., the downstream of a red traffic light is empty. Thus, an appropriate model should define a solution to the Riemann problem with an initial state or both initial states at the vacuum. The latter case is trivial: the Riemann solution remains at the vacuum. The cases with only one initial state at the vacuum are explored next.

4.8.1. Upstream vacuum state. One studies the Lax curves emanating from the vacuum $u_0 = (0, 0)$. By the Rankine–Hugoniot condition,

$$\rho_1 = 0, \quad \sigma = V_2(\rho_2) \qquad \text{or} \qquad \rho_2 = 0, \quad \sigma = V_1(\rho_1).$$

These give 1-shock curves along the ρ_2-axis, and 2-shock curves along the ρ_1-axis.

Hence, in the case connecting the vacuum on the left to $u^+ \in \mathcal{D}_1$, the shock solution first connects to an intermediate state on the ρ_2-axis with a 1-shock curve that coincides with the ρ_2-axis. A physical interpretation of this case is to consider a road with a queue of both large and small vehicles at the downstream, and an empty road at the upstream. By the definition of velocity function (see Figure 1(a)), the smaller vehicles possess a higher velocity for the same total occupied space r. Thus, after a short period of time, only the larger vehicle class ρ_2 is observable at the back of the queue because the first vehicle class overtakes them; i.e., $\rho_1^* = 0$ and $\rho_2^* > 0$. Therefore, starting from a vacuum state on the left, the Lax shock curves always travel along the ρ_2-axis and connect with the slower class. Furthermore, one checks that the shock speed of the 1-shock wave is the same as that predicted by the LWR model.

4.8.2. Downstream vacuum state. Based on the discussion in section 4.3, 1-rarefaction curves connect to the vacuum along the boundaries $\rho_1 = 0$ and $\rho_2 = 0$. Thus, the solution to the case with $u^- \in \mathcal{D}_3$ is clear, where u^- is connected with the vacuum along the boundaries $\rho_1 = 0$ and $\rho_2 = 0$. It remains to discuss the case when $u^- \in \mathcal{D}_1 \backslash \mathcal{D}_3$.

By the features of Lax rarefaction curves (see section 4.3), 1-rarefaction curves are monotonic, convex, and exit from the $\rho_2 = 0$ boundary. Thus, u^- first connects to an intermediate state on the ρ_1-axis via a 1-rarefaction curve. This also has a clear physical interpretation. As two vehicle classes flow into an empty road, the smaller vehicle class ρ_1 advances to the front of the traffic, since it possesses higher speed for the same total occupied space r (see Figure 1(a)). Thus, the intermediate state u^* that connects to the vacuum on the downstream contains only vehicles of the first class. Moreover, the u^* and u^+ are connected along the ρ_1-axis.

4.8.3. Riemann solver at vacuum. The Riemann solver for the vacuum problem is summarized as follows.

Case 1: u^- is at the vacuum (shock solution):

1. $\rho_1^+ > 0,\ \rho_2^+ > 0$. This is a shock solution that connects u^- to $u^* = (0, \rho_2^*)$ by a 1-shock curve along the boundary $\rho_1 = 0$, with $\rho_1^+ + \rho_2^+ > \rho_2^* > \rho_2^+$, then connects u^* and u^+ with a 2-shock curve.
2. $\rho_1^+ = 0,\ \rho_2^+ > 0$. The solution simplifies to a single 1-shock curve that connects u^- with u^+ along the ρ_2-axis.
3. $\rho_1^+ > 0,\ \rho_2^+ = 0$. The intermediate state u^* coincides with the vacuum. Hence, u^- and u^+ are connected by a 2-shock curve along the ρ_1-axis.

Case 2: u^+ is at the vacuum (rarefaction solution):

1. $\rho_1^- > 0,\ \rho_2^- > 0$. In this case, the intermediate state appears on the ρ_1-axis; i.e., $u^* = (\rho_1^*, 0)$ with $\rho_1^- + \rho_2^- > \rho_1^* > 0$. Thus, the Riemann solution first links u^- and u^* with 1-rarefaction, and then connects u^* and the vacuum state along the ρ_1-axis.
2. $\rho_1^- = 0,\ \rho_2^- > 0$, or $\rho_1^- > 0,\ \rho_2^- = 0$. The left state u^- connects to the vacuum on the right-hand side directly via 1-rarefaction curves.

Case 3: Both initial states are at the vacuum. The solution remains at the vacuum.

4.8.4. Stability near the vacuum. The stability of the Riemann solver with initial data near the vacuum is briefly discussed. Riemann solutions are constructed for a left state perturbed away from the vacuum, and a fixed right state.

1. u^- is perturbed to the ρ_2-axis, $\rho_1^- = 0,\ 1 \gg \rho_2^- > 0$. The Riemann solution is composed of a 1-shock curve that connects u^- to $u^* = (0, \rho_2^*)$ with $\rho_1^+ + \rho_2^+ > \rho_2^* > \rho_2^-$ along the ρ_2-axis, and then a 2-shock curve that connects u^* to u^+.
2. u^- is perturbed into the interior of $\mathcal{D}_1$; i.e., $u^- \in \mathcal{D}_1 \backslash \mathcal{D}_3,\ 1 \gg \rho_1^- > 0,\ 1 \gg \rho_2^- > 0$. In this case, the 1-shock curve is slightly shifted away from the ρ_2-axis. The structure of the solver is similar to the previous case, and the deviation between these two solutions is small.
3. u^- is perturbed to the ρ_1-axis, $1 \gg \rho_1^- > 0,\ \rho_2^- = 0$. This gives an intermediate state $u^* = (\rho_1^*, 0)$ with $\rho_1^* > \rho_1^+ + \rho_2^+$. First, u^- connects to u^* along a 1-shock curve that coincides with the ρ_1-axis. Second, u^* connects to u^+ via a 2-rarefaction curve.

In the third case, the 1-shock wave has a larger amplitude than the previous two cases, and the 2-shock wave is replaced by a 2-rarefaction wave. Thus, the structure of the Riemann solution changes for a small perturbation of the Riemann data. This may result in a loss of the continuous dependence on the initial data. Consequently, it is possible to lose well-posedness when the vacuum is involved. Due to the difficulty of obtaining explicit solutions to the Riemann problems, the well-posedness of the creeping model in the presence of the vacuum is an open question.

5. Numerical simulations.

5.1. Numerical method. This section is devoted to illustrating the creeping model (3.5) in numerical simulations, using the Godunov method [18, 26]. The update rule is given explicitly as

$$\begin{pmatrix} \rho_{1,i}^{n+1} \\ \rho_{2,i}^{n+1} \end{pmatrix} = \begin{pmatrix} \rho_{1,i}^{n} \\ \rho_{2,i}^{n} \end{pmatrix} - \frac{\Delta t}{\Delta x} \left(\begin{pmatrix} (\mathcal{F}_1)_{i+\frac{1}{2}}^n \\ (\mathcal{F}_2)_{i+\frac{1}{2}}^n \end{pmatrix} - \begin{pmatrix} (\mathcal{F}_1)_{i-\frac{1}{2}}^n \\ (\mathcal{F}_2)_{i-\frac{1}{2}}^n \end{pmatrix} \right), \tag{5.1}$$

where Δx and Δt are sizes of the space and time step, and $\rho_{j,i}^n$ represents the density of the jth class in the ith cell at time $t = n\Delta t$. Moreover, $(\mathcal{F}_j)_{i-\frac{1}{2}}^n$ and $(\mathcal{F}_j)_{i+\frac{1}{2}}^n$ are numerical fluxes through the upstream and downstream boundaries of the ith cell for the jth vehicle class at time $t = n\Delta t$. These fluxes are obtained by explicitly analyzing the sending and receiving potential for each vehicle class as an analogy to the *cell transmission model* (CTM) [11]. Note that the CTM can be viewed as a special case of (5.1) where only one vehicle class is present, i.e., a discretized version of the LWR model.

In order to develop the new numerical scheme, it is helpful to review the key elements of the CTM as follows:

1. The evolution equation of the CTM is
$$\rho_i^{n+1} = \rho_i^n + \frac{\Delta t}{\Delta x}\left(\mathcal{F}_{i-1/2}^n - \mathcal{F}_{i+1/2}^n\right),$$
where ρ_i^{n+1} is the traffic density of the ith cell at the next time step $t = (n+1)\Delta t$ and $\mathcal{F}_{i-1/2}^n$ and $\mathcal{F}_{i+1/2}^n$ are the inflow and outflow of cell i over the time interval $t = n\Delta t$ to $t = (n+1)\Delta t$.
2. The cell inflow and outflow $\mathcal{F}_{i-1/2}^n$ and $\mathcal{F}_{i+1/2}^n$ are each determined by taking the minimum of the vehicles available to be sent from the cell upstream of the boundary and the vehicles available to be received by the cell downstream of the boundary:
$$\mathcal{F}_{i-1/2}^n = \min\left\{S(\rho_{i-1}^n)\ ,\ R(\rho_i^n)\right\}, \qquad \mathcal{F}_{i+1/2}^n = \min\left\{S(\rho_i^n)\ ,\ R(\rho_{i+1}^n)\right\},$$
where $S(\cdot)$ and $R(\cdot)$ are known as the sending and receiving functions.
3. The sending and receiving functions are defined based on the flux function $Q(\rho) = \rho V(\rho)$ of an LWR model:
$$S(\rho) = \begin{cases} Q(\rho) & \text{if } \rho \le \rho_c, \\ Q^{\max} & \text{if } \rho > \rho_c, \end{cases} \qquad R(\rho) = \begin{cases} Q^{\max} & \text{if } \rho \le \rho_c, \\ Q(\rho) & \text{if } \rho > \rho_c, \end{cases} \tag{5.2}$$
where ρ_c denotes the critical density where the maximum flux $Q^{\max}$ is obtained. One sees that $S(\cdot)$ gives the maximum possible flow that can be sent from the upstream cell given the upstream density, and $R(\cdot)$ defines the maximum flow that can be received in the downstream cell given the downstream density.

In [29], a generalization of the CTM to homogeneous multiclass models is proposed. Here, a scheme for a heterogeneous extension of the CTM is developed. Following the CTM framework, the cell boundary flow is the minimum of the sending and receiving functions, with the extension that the sending and receiving functions are defined for each vehicle class. For simplicity, the initial states of the upstream and downstream cells are represented as $u^- = (\rho_1^-, \rho_2^-)$ and $u^+ = (\rho_1^+, \rho_2^+)$. The flows of the two vehicle classes over a cell boundary are determined as

$$\mathcal{F}_1 = \min\left\{S_1(\rho_1^-, \rho_2^-),\ R_1(\rho_1^+, \rho_2^+)\right\}, \quad \mathcal{F}_2 = \min\left\{S_2(\rho_1^-, \rho_2^-),\ R_2(\rho_1^+, \rho_2^+)\right\}, \tag{5.3}$$

where $S_j(\cdot)$ and $R_j(\cdot)$, $j = 1, 2$, represent the sending and receiving functions of the two vehicle classes.

5.1.1. Sending and receiving functions for ρ_1. The flux function of the first vehicle class is defined as

$$Q_1(\rho_1, \rho_2) = \rho_1 V_1(\rho_1 + \rho_2). \tag{5.4}$$

The sending and receiving functions of the first vehicle class are defined as

$$S_1(\rho_1^-,\rho_2^-)=\begin{cases} Q_1(\rho_1^-,\rho_2^-) & \text{if } \rho_1^- \le \rho_1^{\mathrm{c}}(\rho_2^-),\\ Q_1^{\max}(\rho_2^-) & \text{if } \rho_1^- > \rho_1^{\mathrm{c}}(\rho_2^-),\end{cases}$$
$$R_1(\rho_1^+,\rho_2^+)=\begin{cases} Q_1^{\max}(\rho_2^+) & \text{if } \rho_1^+ \le \rho_1^{\mathrm{c}}(\rho_2^+),\\ Q_1(\rho_1^+,\rho_2^+) & \text{if } \rho_1^+ > \rho_1^{\mathrm{c}}(\rho_2^+),\end{cases}$$

where $Q_1^{\max}(\rho_2)=\max_{\rho_1}\{Q_1(\rho_1,\rho_2)\}$ is the maximum of (5.4) and $\rho_1^{\mathrm{c}}(\rho_2)=\frac{r_1^{\mathrm{m}}-\rho_2}{2}$ is the critical density of ρ_1 such that $Q_1^{\max}$ is obtained.

5.1.2. Sending and receiving functions for ρ_2. The second vehicle class is stationary in the creeping phase $\mathcal{D}_2$. To capture creeping, the flux function of the second vehicle class is extended in the following way:

$$Q_2(\rho_1,\rho_2)=\max\{\rho_2 V_2(\rho_1+\rho_2),0\}.$$

The sending and receiving functions for ρ_2 become

$$S_2(\rho_1^-,\rho_2^-)=\begin{cases} Q_2(\rho_1^-,\rho_2^-) & \text{if } \rho_2^- \le \rho_2^{\mathrm{c}}(\rho_1^-),\\ Q_2^{\max}(\rho_1^-) & \text{if } \rho_2^- > \rho_2^{\mathrm{c}}(\rho_1^-),\end{cases}$$
$$R_2(\rho_1^+,\rho_2^+)=\begin{cases} Q_2^{\max}(\rho_1^+) & \text{if } \rho_2^+ \le \rho_2^{\mathrm{c}}(\rho_1^+),\\ Q_2(\rho_1^+,\rho_2^+) & \text{if } \rho_2^+ > \rho_2^{\mathrm{c}}(\rho_1^+),\end{cases}$$

where $Q_2^{\max}(\rho_1)=\max_{\rho_2}\{Q_2(\rho_1,\rho_2)\}$ and $\rho_2^{\mathrm{c}}(\rho_1)=\frac{r_2^{\mathrm{m}}-\rho_1}{2}$ is the critical density of the second vehicle class such that $Q_2^{\max}$ is obtained.

It can be shown that the numerical scheme (5.1) generates numerical fluxes that are consistent with those given by the Riemann solver. In $\mathcal{D}_1$, by checking the propagating directions of shock or rarefaction waves predicted by the model (3.5), the flux through each cell boundary is consistent with that predicted by the numerical scheme (5.3) based on the sending and receiving of vehicles. In $\mathcal{D}_2$, (5.1) collapses to the CTM [11]. Furthermore, it can be verified that the numerical solver is consistent with the creeping model with phase transitions, e.g., $\mathcal{F}_2=0$, if $u^+\in\mathcal{D}_2$.

To avoid interactions of waves from neighboring Riemann problems, the time step should satisfy the CFL condition: $v^{\mathrm{m}}\frac{\Delta t}{\Delta x}\le 1$.

5.2. Numerical simulations and comparisons. Numerical simulations are performed to illustrate the properties of the creeping model, and the results are compared with those of the n-populations model [4] with two vehicle classes. For these numerical tests, the parameters for the two models are selected such that the maximums of the maximum velocities and effective jam densities of two vehicle classes are the same. Hence, the following parameters for the creeping model are used:

$$v_1^{\mathrm{m}}=v_2^{\mathrm{m}}=1.8 \quad \text{and} \quad r_1^{\mathrm{m}}=1.8,\quad r_2^{\mathrm{m}}=1.0.$$

In the n-populations model, let

$$v_1^{\mathrm{m}}=1.8,\quad v_2^{\mathrm{m}}=1.0,\quad \text{and} \quad r_1^{\mathrm{m}}=r_2^{\mathrm{m}}=1.8.$$

Here, v_1^{m} and v_2^{m} are the maximum velocities, and r_1^{m} and r_2^{m} are the maximum occupied spaces of the two vehicle classes.

Note that both models provide the freedom to choose model parameters. For instance, the creeping model is able to capture creeping as long as the maximum

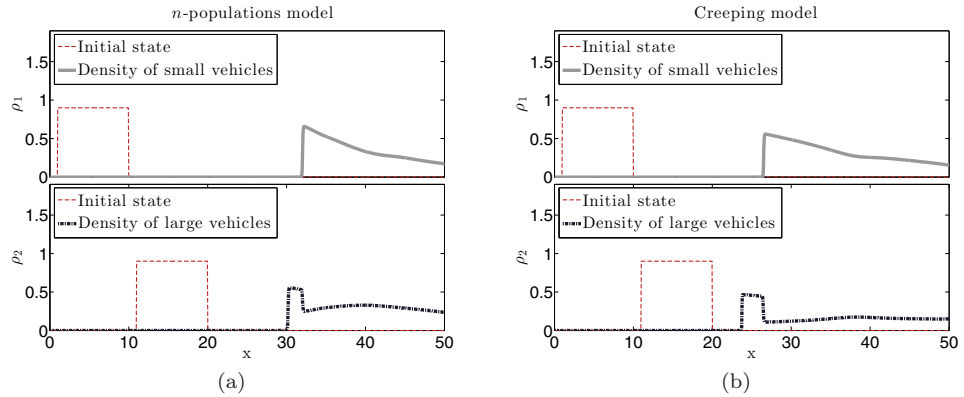

FIG. 3. *Example* 1: *An experiment of overtaking.* (a) *The traffic state of the n-populations model at* $t = 50$*;* (b) *the numerical results of the creeping model at* $t = 33$*. In each figure, the densities of the first vehicle class (thick-solid-gray) and the second vehicle class (thick-dashed-black), together with the initial condition (thin-dashed-red), are shown.*

velocity is unique and the maximum occupied spaces are distinct. This is desirable since one can adjust these parameters when traffic data is available for calibration. In order to highlight the properties of the creeping model, the gap between the maximum occupied spaces of two vehicle classes is made large enough to generate more clear creeping behaviors.

Furthermore, the computational domain is chosen as $x \in [0, 50]$, with $\Delta x = 0.05$, and the time step Δt is chosen based on the CFL condition $\Delta t = \Delta x / v^{\mathrm{m}}$, where $v^{\mathrm{m}} = \max\{v_1^{\mathrm{m}}, v_2^{\mathrm{m}}\}$.

5.2.1. Example 1: Overtaking. In this test, the larger vehicle class ρ_2 is in front of the smaller class ρ_1 at $t = 0$. The initial condition for both vehicle classes is given as follows:

$$\rho_1(x,0) = \begin{cases} 0.9 & \text{if } x \in [1,10], \\ 0 & \text{otherwise,} \end{cases} \qquad \rho_2(x,0) = \begin{cases} 0.9 & \text{if } x \in [11,20], \\ 0 & \text{otherwise.} \end{cases}$$

On the boundaries, assume that the upstream inflow is zero, and vehicles are allowed to flow out of the study area freely; i.e., the downstream of the study region is empty.

As time evolves, the small vehicle class overtakes the large class. Both the n-populations model [4] and the creeping model (3.5) exhibit overtaking (see Figure 3), although it is initiated at different times due to the structures of the two models and the selected parameters. For the n-populations model, one can clearly observe that all small vehicles have overtaken the large vehicles at $x = 31$ by $t = 50$. A similar overtaking result is observed at $x = 26$ and $t = 33$ in the creeping model. Note that in the creeping model all traffic states remain in $\mathcal{D}_1$.

5.2.2. Example 2: Creeping. The next example depicts a scenario when two vehicle classes approach a red traffic light. Here, the same model parameters are applied as in Example 1, but a new initial condition is given as follows:

$$\rho_1(x,0) = \begin{cases} 0.7 & \text{if } x \in [1,19], \\ 0 & \text{otherwise,} \end{cases} \qquad \rho_2(x,0) = \begin{cases} 0.7 & \text{if } x \in [20,50], \\ 0 & \text{otherwise.} \end{cases}$$

The initial condition again describes the situation where the small vehicle class starts behind the larger vehicles. For the boundary conditions, the upstream inflow is set

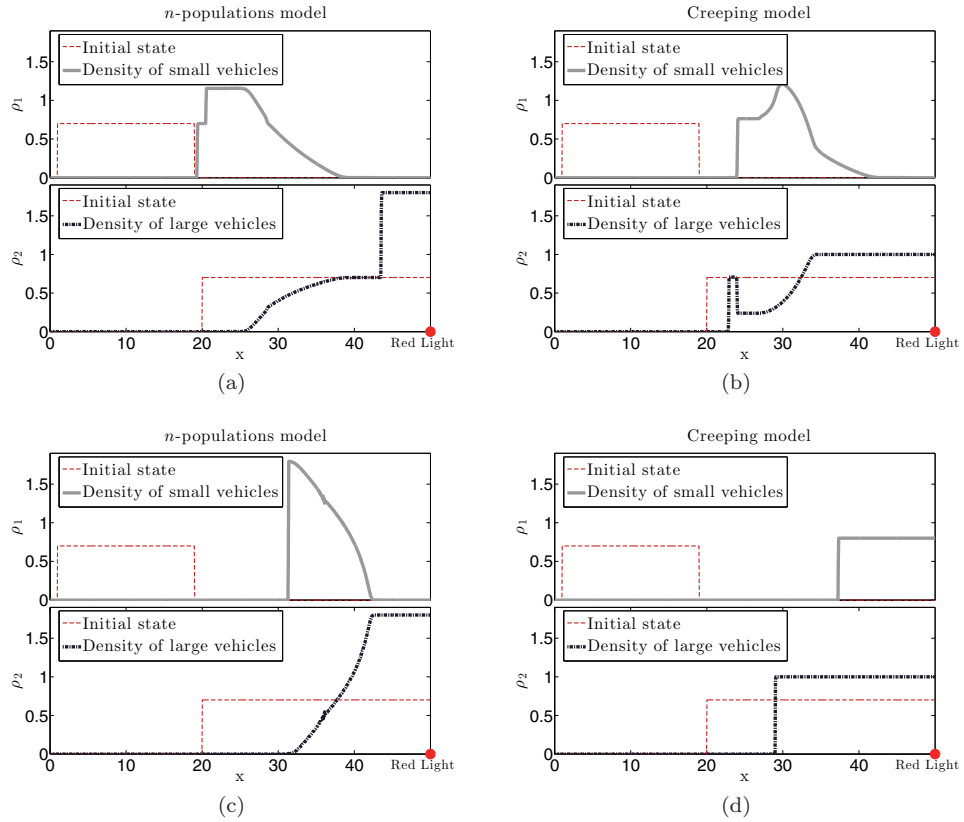

FIG. 4. *Example* 2: *An experiment with creeping.* (a) *and* (c) *are the simulation results of the* n*-populations model at* $t = 33$ *and* $t = 150$*, respectively.* (b) *and* (d) *exhibit the results of the creeping model at* $t = 33$ *and* $t = 150$*, respectively.*

to zero, so that no new vehicles enter the domain. The downstream outflow for both vehicle classes is also set to zero to model a red traffic light. Example 2 is suitable to illustrate the main difference between the n-populations model [4] and the creeping model (see Figure 4).

Initially, the larger vehicle class is in front of the smaller vehicle class at a total occupied space below the maximum occupied space. At time $t = 33$, overtaking is observable in both models (see Figures 4(a), 4(b)), where the smaller vehicle class catches up and competes for free spaces with the larger vehicle class. For the larger vehicle class, shock waves are triggered from the right boundary and travel backwards into the computational domain, and large vehicles accumulate at the traffic light in both models.

In the n-populations model, a unique stationary point for both vehicle classes is assumed at $r^{\mathrm{m}} = 1.8$. Thus, the small vehicles that arrive at the end of the stationary queue composed of large vehicles cannot advance by creeping since the space has been completely occupied by large vehicles (see Figure 4(a)). In contrast, the creeping model uses different maximum occupied spaces for the two vehicle classes. As a result, the large vehicle class that arrives at the red traffic light earlier reaches the stationary point of its own class, i.e., $r_2^{\mathrm{m}} = 1.0$ (see Figure 4(b)), but small vehicles may still advance.

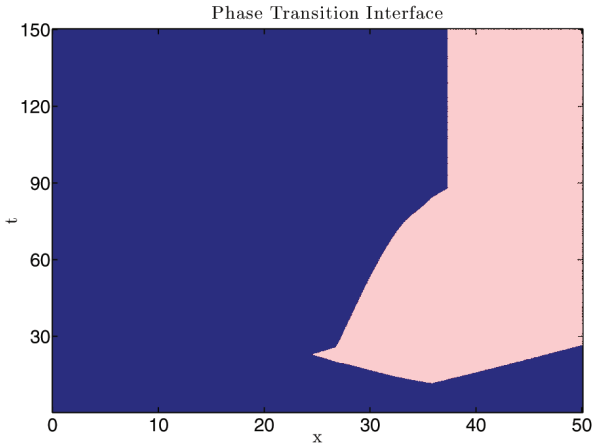

FIG. 5. *Phase transition interface in the time-space plane for Example* 2. *The light-red region denotes the creeping phase, while the dark-blue region is the noncreeping phase.*

At time $t = 13$, the front of the small vehicle class begins to meet the end of the stationary queue of the large vehicle class located around $x = 35$. At this point, a phase transition occurs from the noncreeping to the creeping phase, and creeping begins to occur (see Figure 5). As the lead vehicle of the creeping class continues to slowly advance, the points in the domain $x > 35$ begin to transition into $\mathcal{D}_2$. Similarly, as the queue of large vehicles continues to grow, and higher densities of small vehicles progress forward, points $x < 35$ also transition to $\mathcal{D}_2$ before eventually transitioning back to D_1 when the creeping vehicles have completely passed.

At $t = 150$, one sees very different configurations of the density profiles in the two models (see Figures 4(c), 4(d)). In the n-populations model, the road segment adjacent to the red traffic light $x \in [42, 50]$ is occupied exclusively by larger vehicles, while traffic on the road segment $x \in [32, 42]$ is composed of two vehicle classes. It is clear that the n-populations model does not allow creeping, while the creeping model allows the smaller vehicles to overtake the second vehicle class even through the larger vehicles are stationary due to the red traffic light. Thus, this test shows that the new model is appropriate to model creeping in a heterogeneous traffic flow.

6. Conclusion. In this work, a new heterogeneous model for two vehicle classes is developed, which is based on the philosophy that vehicles with different sizes occupy different spaces on the roadway. The model is designed to capture the creeping scenario when large vehicles are stopped while smaller vehicles continue to move. To achieve this goal, velocity functions are introduced that have the same maximum velocity but distinct maximum occupied spaces. The model is described as a phase transition model where a 2×2 system reduces to the LWR model as the occupied space increases above a critical point r_2^{m}. A Riemann solver is defined across the phase transition. Finally, numerical tests based on the finite volume Godunov scheme are performed, and comparisons between the creeping model and the two class n-populations model are carried out. These tests show that the creeping model can not only describe overtaking behavior, but also model the dynamics of creeping in heterogeneous flow.

REFERENCES

[1] F. Ancona and A. Marson, *Existence theory by front tracking for general nonlinear hyperbolic systems*, Arch. Ration. Mech. Anal., 185 (2007), pp. 287–340.

[2] A. Aw and M. Rascle, *Resurrection of "second order" models of traffic flow*, SIAM J. Appl. Math., 60 (2000), pp. 916–938.

[3] P. Baiti and H. K. Jenssen, *Well-posedness for a class of* 2×2 *conservation laws with* L^∞ *data*, J. Differential Equations, 140 (1997), pp. 161–185.

[4] S. Benzoni-Gavage and R. M. Colombo, *An n-populations model for traffic flow*, Eur. J. Appl. Math., 14 (2003), pp. 587–612.

[5] F. Berthelin, P. Degond, M. Delitala, and M. Rascle, *A model for the formation and evolution of traffic jams*, Arch. Ration. Mech. Anal., 187 (2008), pp. 185–220.

[6] S. Blandin, D. Work, P. Goatin, B. Piccoli, and A. Bayen, *A general phase transition model for vehicular traffic*, SIAM J. Appl. Math., 71 (2011), pp. 107–127.

[7] A. Bressan, *Hyperbolic Systems of Conservation Laws—The One Dimensional Cauchy Problem*, Oxford University Press, Oxford, UK, 2000.

[8] A. Bressan and R. M. Colombo, *The semigroup generated by* 2×2 *conservation laws*, Arch. Ration. Mech. Anal., 133 (1995), pp. 1–75.

[9] R. M. Colombo, *Hyperbolic phase transitions in traffic flow*, SIAM J. Appl. Math., 63 (2002), pp. 708–721.

[10] R. M. Colombo, P. Goatin, and F. S. Priuli, *Global well posedness of traffic flow models with phase transitions*, Nonlinear Anal., 66 (2007), pp. 2413–2426.

[11] C. F. Daganzo, *The cell transmission model: A dynamic representation of highway traffic consistent with the hydrodynamic theory*, Transportation Res. Part B, 28 (1994), pp. 269–287.

[12] C. F. Daganzo, *A continuum theory of traffic dynamics for freeways with special lanes*, Transportation Res. Part B, 31 (1997), pp. 83–102.

[13] C. F. Daganzo, *A behavioral theory of multi-lane traffic flow. Part* I: *Long homogeneous freeway sections*, Transportation Res. Part B, 36 (2002), pp. 131–158.

[14] S. Fan, M. Herty, and B. Seibold, *Comparative model accuracy of a data-fitted generalized Aw-Rascle-Zhang model*, Netw. Heterog. Media, 9 (2014), pp. 239–268.

[15] S. Fan and B. Seibold, *A Comparison of Data-Fitted First Order Traffic Models and Their Second Order Generalizations via Trajectory and Sensor Data*, Paper 13–4853, Transportation Research Board, Washington, DC, 2013.

[16] M. Garavello and B. Piccoli, *Source-destination flow on a road network*, Comm. Math. Sci., 3 (2005), pp. 261–283.

[17] J. Glimm, *Solutions in the large for nonlinear hyperbolic systems of equations*, Comm. Pure Appl. Math., 18 (1965), pp. 697–715.

[18] S. K. Godunov, *A difference scheme for the numerical computation of a discontinuous solution of the hydrodynamic equations*, Math. Sb., 47 (1959), pp. 271–306.

[19] B. D. Greenshields, *A study of traffic capacity*, Proc. Highway Res. Record, 14 (1935), pp. 448–477.

[20] D. Hoff, *Invariant regions for systems of conservation laws*, Trans. Amer. Math. Soc., 289 (1985), pp. 591–610.

[21] W. L. Jin, *A multi-commodity Lighthill-Whitham-Richards model of lane-changing traffic flow*, Procedia Soc. Behav. Sci., 80 (2013), pp. 658–677.

[22] B. L. Keyfitz and H. C. Kranzer, *A system of non-strictly hyperbolic conservation laws arising in elasticity theory*, Arch. Ration. Mech. Anal., 72 (1980), pp. 219–241.

[23] P. D. Lax, *Hyperbolic systems of conservation laws* II, Comm. Pure Appl. Math., 10 (1957), pp. 537–566.

[24] P. G. Le Floch, *Hyperbolic Systems of Conservation Laws: The Theory of Classical and Nonclassical Shock Waves*, Birkhäuser, Cambridge, MA, 2002.

[25] J. P. Lebacque, S. Mammar, and H. Haj-Salem, *Generic Second Order Traffic Flow Modelling*, in Transportation and Traffic Theory, R. E. Allsop, M. G. H. Bell, and B. G. Heydecker, eds., Proceedings of the 17th International Symposium on Transportation and Traffic Theory (ISTTT), Elsevier, New York, 2007, pp. 755–776.

[26] R. J. LeVeque, *Finite Volume Methods for Hyperbolic Problems*, Cambridge University Press, Cambridge, UK, 2002.

[27] M. J. Lighthill and G. B. Whitham, *On kinematic waves.* II. *A theory of traffic flow on long crowded roads*, Proc. Roy. Soc. A, 229 (1955), pp. 317–345.

[28] T. P. Liu and T. Yang, *Weak solutions of general systems of hyperbolic conservation laws*, Comm. Math. Phys., 230 (2002), pp. 289–327.

[29] S. Logghe and L. H. Immers, *Heterogeneous traffic flow modelling with the LWR model using passenger-car equivalents*, in Proceedings of the 10th World Congress on ITS, Madrid, Spain, 2003; available online at http://www.kuleuven.be/traffic/dwn/P2003E.pdf.
[30] S. Logghe and L. H. Immers, *Multi-class kinematic wave theory of traffic flow*, Transportation Res. Part B, 42 (2008), pp. 523–541.
[31] R. Nair, H. S. Mahmassani, and E. Miller-Hooks, *A porous flow approach to modeling heterogeneous traffic in disordered systems*, Transportation Res. Part B, 45 (2011), pp. 1331–1345.
[32] D. Ngoduy and R. Liu, *Multiclass first-order simulation model to explain non-linear traffic phenomena*, Phys. A, 385 (2007), pp. 667–682.
[33] P. I. Richards, *Shock waves on the highway*, Oper. Res., 4 (1956), pp. 42–51.
[34] S. Smulders, *Control of freeway traffic flow by variable speed signs*, Transportation Res. Part B, 24 (1990), pp. 111 – 132.
[35] J. W. C. van Lint, S. P. Hoogendoorn, and M. Schreuder, *Fastlane: New multiclass first-order traffic flow model*, Transport. Res. Record, 2088 (2008), pp. 177–187.
[36] G. C. K. Wong and S. C. Wong, *A multi-class traffic flow model—An extension of LWR model with heterogeneous drivers*, Transportation Res. Part A, 36 (2002), pp. 827–841.
[37] H. M. Zhang, *A non-equilibrium traffic model devoid of gas-like behavior*, Transport. Res. Part B, 36 (2002), pp. 275–290.
[38] H. M. Zhang and W. L. Jin, *Kinematic wave traffic flow model for mixed traffic*, Transport. Res. Record, 1802 (2002), pp. 197–204.
[39] P. Zhang, R. X. Liu, S. C. Wong, and S. Q. Dai, *Hyperbolicity and kinematic waves of a class of multi-population partial differential equations*, Eur. J. Appl. Math., 17 (2006), pp. 171–200.
[40] Z. Zhu and T. Wu, *Two-phase fluids model for freeway traffic flow and its application to simulate evolution of solitons in traffic*, J. Transport. Eng., 129 (2002), pp. 51–56.